Asociación Argentina
de Mecánica Computacional

Mecánica Computacional Vol XLII, pp. 647-654
A. Caggiano, G. Etse, P. Folino, M. Goldschmit, M. Pucheta, M. Storti (Eds.)
P. Folino, M. Ripani, S. Vrech (Issue eds.)
Buenos Aires, November 11-14, 2025

# MEMS SENSORS IN STRUCTURAL HEALTH MONITORING: APPLICATIONS WITH 3D-PRINTED MATERIALS

**Mariana H. Padilha[a], Maurício da S. R. Mombach[a], Leandro F. Friedrich[a], Vicente B. Puglia[a], Mikael da Cruz[a], Alessandro G. Girardi[a] e Ignacio Iturrioz[b].**

[a] *Postgraduate Program in Engineering, Universidade Federal do Pampa, Av. Tiaraju 810, CEP 97546-550, Alegrete, Brazil. marianapadilha.aluno@unipampa.edu.br; mauriciomombach.aluno@unipampa.edu.br; leandrofriederich@unipampa.edu.br; vicentepuglia@unipampa.edu.br; mikaelcruz.aluno@unipampa.edu.br; alessandro.girardi@unipampa.edu.br.*

[b] *Mechanical Post-Graduate Program, Universidade Federal do Rio Grande do Sul, Sarmento Leite 425, CEP 90050-170, Porto Alegre, Brazil. ignacio@mecanica.ufrgs.br.*

**Keywords:** MEMS sensors, Acoustic Emission, Structural Health Monitoring, b-value analysis, Natural Time analysis, Crack propagation

**Abstract:** This study presents an acoustic emission (AE) monitoring strategy based on MEMS (Micro-Electro-Mechanical Systems) sensors applied to 3D-printed structures. AE data were analyzed using the b-value method to track damage development and Natural Time (NT) analysis to identify the onset of critical conditions. A comparison with a commercial piezoelectric sensor revealed similar performance, with both sensors detecting a reduction in the b-value preceding failure. MEMS sensors demonstrated an enhanced capacity to capture high-frequency signals. These results underline the potential of MEMS sensors as cost-effective tools for structural health monitoring in additive manufacturing contexts.

ISSN: 2591-3522 DOI: 10.70567/mc.v42.ocsid8460

# 1. INTRODUCTION

Acoustic Emission (AE) is a sensitive non-destructive technique used to detect internal structural changes such as crack initiation and propagation. Conventional AE systems utilize piezoelectric sensors due to their precision and robustness, but their size and cost limit their use in embedded or distributed systems. MEMS sensors, in contrast, offer low-cost, miniaturized alternatives suitable for scalable monitoring applications [1,2]. Despite promising advantages, MEMS sensors are still under exploration for AE applications, requiring validation against established commercial devices [2,3]. This work evaluates MEMS sensors in a comparative experimental framework, using 3D-printed polymer specimens subjected to three-point bending tests. Both a commercial piezoelectric sensor and a MEMS sensor were used to capture AE signals. The AE signals were analyzed by using the b-value, commonly used in seismology [4] to identify damage evolution, and Natural Time analysis to detect criticality conditions.

# 2. AE DATA ANALYSIS

The b-value analysis in Acoustic Emission (AE) originates from seismological studies, particularly the Gutenberg-Richter law [4], which describes the statistical relationship between the magnitude of events and their cumulative frequency. Adapted for AE monitoring, the b-value represents the slope in the log-log plot between AE signal amplitude and the cumulative number of events [6,7], the law can be expressed as follows:

$$N(\geq A) = \zeta A^{-b} \tag{1}$$

Where $N(\geq A)$ is the cumulative number of AE events with amplitude $\geq A$, $\zeta$ is a normalization constant, Ais the amplitude of the AE signal and b is the b-value, which reflects damage state. This parameter is considered a universal law, independent of system scale, as discussed by Shiotani et al. (1994). According to Aki (1967) and Carpinteri et al. (2009), the b-value is associated with the fractal dimension D of the crack distribution region, via the expression $D = 2b$, in early damage stages, AE events are typically generated by microcracks distributed in three dimensions ($D \approx 3 \rightarrow b \approx 1.5$), which results in many low-amplitude signals. As damage evolves, the events become more localized, forming clusters that lead to macrocrack formation. In this final stage, damage concentrates on a surface ($D \approx 2 \rightarrow b \approx 1.0$), corresponding to a higher proportion of large-amplitude events. Thus, a progressive decrease in the b-value indicates damage localization and acts as a precursor to structural failure. In this study, the b-value was dynamically computed using a moving window approach, allowing temporal tracking of localized damage development. Figure 1(a) illustrates the typical variation of the $b$-value during the damage process. Monitoring how the $b$-value changes over time provides insight into when and where damage localization begins within the structure.

## 2.2 Natural Time Analysis

The analysis in the natural time domain allows identifying critical states in complex systems [11]. More specific, the natural time $\chi_k$ of the $k$-th event is defined as the normalized occurrence of that event, obtained by dividing it by the total number of considered events, $N$, that is $\chi_k = k/N$ (see Figure 1(b)). Simultaneously, natural time $\chi_k$ serves as an index for the timing of the $k$-th event. It inherently falls within the range of (0,1) [12]. Let $Q_k$ represents a quantity proportional to the energy of the individual $k$ -th event, with its normalized energy expressed as $p_k = Q_k \big/ \sum_{n=1}^{N} Q_n$ . Therefore, in natural time analysis, the evolution of the pair $(\chi_k, p_k)$ is considered, as showed in Figure 1(b) [12].

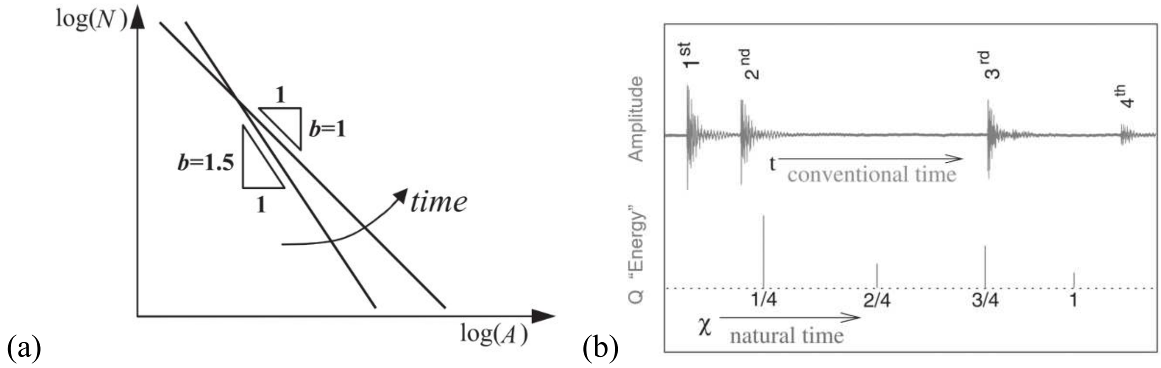

Figure 1: (a) The *b*-value evolution in experimental test [10] and, (b) Natural time in the context of acoustic emission time series.

Using the sequence of pairs ($\chi_k$, $p_k$), two key order parameters are evaluated: (1) Natural Time Variance ($\kappa_1$):

$$\kappa_1 = \langle \chi^2 \rangle - \langle \chi \rangle^2 \equiv \sum_{k=1}^{N} p_k \left(\frac{k}{N}\right)^2 - \left(\sum_{k=1}^{N} \frac{k}{N} p_k\right)^2 \tag{2}$$

This parameter identifies the proximity of the system to a critical state. According to Varotsos et al., the system is said to be near criticality when: $\kappa_1 \rightarrow 0.070$.

(2) Average Spectral Distance (D): To evaluate the spectral deviation from a theoretical reference, the power spectrum $\Pi(\omega)$ is calculated.

$$\Pi(\omega) = \left| \sum_{k=1}^{N} p_k e^{i\omega \frac{k}{N}} \right|^2 \tag{3}$$

Where $\omega = 2\pi\phi$ ( $\phi \in (0, 0.5)$ standing for the frequency in natural time) and the ideal normalized power spectrum,

$$\Pi(\omega)_{ideal} = \frac{18}{5\omega^2} - \frac{6\cos\omega}{5\omega^2} - \frac{12\sin\omega}{5\omega^3} \tag{4}$$

If $\omega \rightarrow 0$, (3) simplifies to $\Pi(\omega)_{ideal} \approx 1 - 0.07\omega^2$ . When $\Pi(\omega)$ approaches $\Pi(\omega)_{ideal}$ from below, the critical state is indicated. Finally, according to Varotsos [11, 12], the dynamical system is defined as in a critical state if:

1) The variance $\kappa_1$, when descending from above, approaches 0.070;

2) The "average" distance $\langle D \rangle$ becomes smaller than $10^2$.

In summary, the NT framework complements b-value analysis by offering enhanced sensitivity to precursory patterns and identifying critical points before macroscopic failure occurs. Together, both methods provide a robust and predictive diagnostic tool for structural health monitoring.

## 3. EXPERIMENTAL PROCEDURE

Flexural tests were conducted on two 3D-printed acrylonitrile butadiene styrene (ABS) samples using a Shimadzu AGS-X universal testing machine with a 5 kN load capacity [9]. Tests followed a three-point bending configuration under displacement control at 0.5 mm/min. The samples, designed in SolidWorks and processed with Creality Slicer, measured 120 × 50 × 30 mm and were printed with a Creality K1c printer. The printing parameters included a 0.4 mm nozzle, 1.75 mm filament, 0.2 mm layer thickness, 0.4 mm line width, 35% infill (line pattern), nozzle speed of 50 mm/s, 240°C hot-end temperature, and 105°C bed temperature. Both specimens shared the same print orientation. Two independent systems were used to acquire AE signals. The commercial setup employed a piezoelectric sensor (PCB model 352C03), connected to a Brüel & Kjær PHOTON+ system, operating at 24.8 kHz. The MEMS-based system used an ADXL1002BCPZ uniaxial accelerometer with a 100 kHz sampling rate. Signal conditioning included a first-order RC filter (R = 63 Ω, C = 100 nF), an MCP3201 ADC, and a Raspberry Pi 4 microcontroller with SPI communication and DMA acquisition. Data was visualized in real time using custom software developed in Python (SonusTrack) shown in Figure 2 (a) and Figure 2 (b).

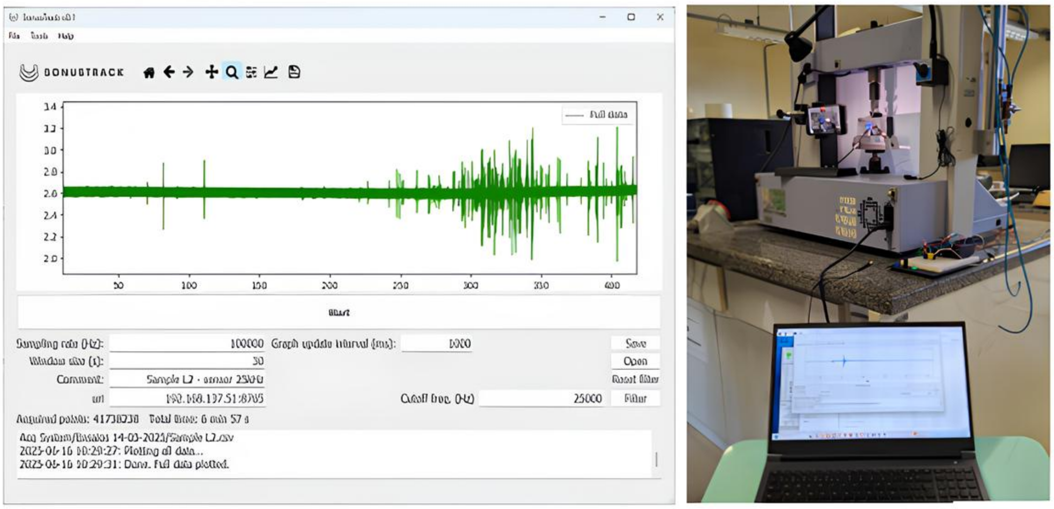

a) b)

Figure 2: (a) Main screen of the software developed for real-time data acquisition, and (b) Complete setup for MEMS accelerometer data acquisition.

## 4. RESULTS

### 4.1 Global Mechanical Response

The mechanical behavior of both printed ABS specimens during the three-point bending tests revealed a consistent response pattern. Figure 3(a) presents the force versus vertical displacement curves, while Figure 3(b) shows the final fracture configurations for both samples.

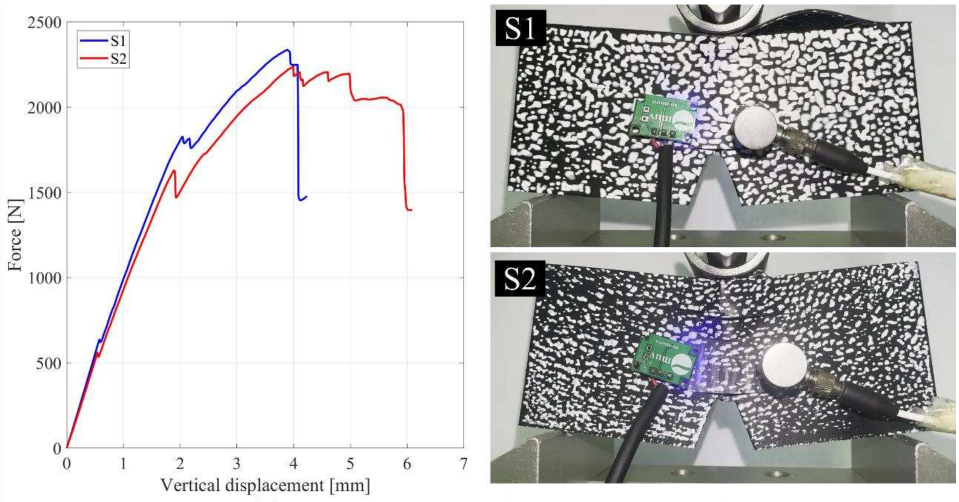

(a) (b)

Figure 3: (a) The force versus vertical displacement curves, (b) The final fracture configurations for both samples (S1) and (S2).

Both curves exhibit distinct points of instability corresponding to abrupt stiffness losses at approximately 0.5 mm and 1.91 mm of vertical displacement. These discontinuities are indicative of delamination or crack nucleation between printed layers—particularly near the notched regions, where stress concentration is naturally higher. Sample 1 failed primarily due to interlayer delamination initiated at the outermost region beneath the loading point. This mode of failure suggests poor interfacial adhesion in this localized zone. In contrast, Sample 2 presented a different behavior: a stable crack propagation originated at the notch and extended toward the upper layer of the specimen, leading to a more gradual post-peak softening. This suggests that the internal filament structure contributed to a more distributed energy dissipation mechanism. Despite these differences in fracture progression, the global load-bearing capacity and stiffness were comparable, highlighting good repeatability in the printing and testing process.

### 4.2 Acoustic Emission Analysis and Sensor Comparison

The AE activity during the bending test of Sample 1 was captured using both the PCB piezoelectric sensor and the MEMS-based system. The data were synchronized using normalized time (t/t*) for comparative analysis. Figure 4(a) shows the cumulative number of AE events detected by each sensor, along with the normalized AE amplitude and the applied load. The event accumulation trends are similar between both systems, although the MEMS sensor captured a broader amplitude range, including high-energy bursts that were not visible in the PCB dataset. This highlights the MEMS sensor's greater sensitivity to energetic fracture events. Figure 4(b) presents a direct comparison of AE waveforms captured by both sensors at approximately t/t* = 0.19. The MEMS signal exhibits denser oscillations and higher frequency components, while the PCB signal appears smoother and more attenuated. The Faster Fourier Transform analysis included in the same figure confirms the wider bandwidth of the MEMS sensor, which recorded significant energy above 9 kHz. This spectral resolution is particularly useful for identifying rapid energy release mechanisms during crack propagation. The evolution of the b-value over time is plotted in Figure 4(c). Both sensors show a similar trend: initially low b-values rise to approximately 1.25 at mid-test, followed by a decline toward the end of the experiment. This pattern reflects the transition from dispersed microcracking to localized macrocrack formation, reinforcing the capability of both sensor types to track damage evolution using statistical AE parameters.

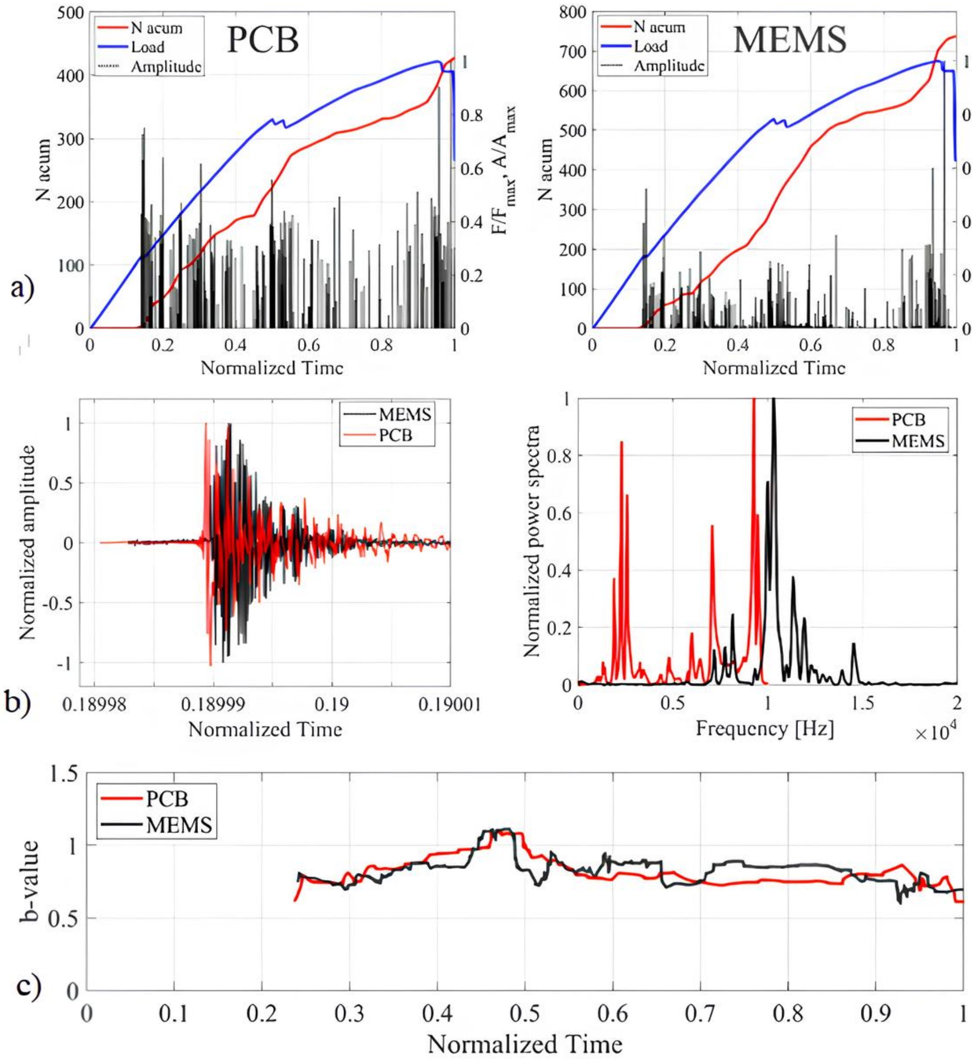

Figure 4: Comparison of the PCB and MEMS sensors: (a) accumulated number of AE signals with the normalized (on the right-hand scale): load, and AE-signal amplitudes (in log scale for the PCB sensor); (b) Signal and FFT comparison; (c) *b*-value.

Natural Time (NT) analysis was also performed using AE signals with energy estimated as $A^{1.5}$. The MEMS-based NT parameters revealed criticality conditions—$\kappa_1$ nearing 0.070 and D below $10^{-2}$—occurring between t/t* = 0.35 and 0.48 shown in Figure 5(b). For the PCB sensor, these conditions were observed later, between t/t* = 0.5 and 0.9 shown in Figure 5(a). These findings suggest that the MEMS sensor provided earlier indications of damage localization and impending failure, demonstrating its potential for real-time structural health diagnostics.

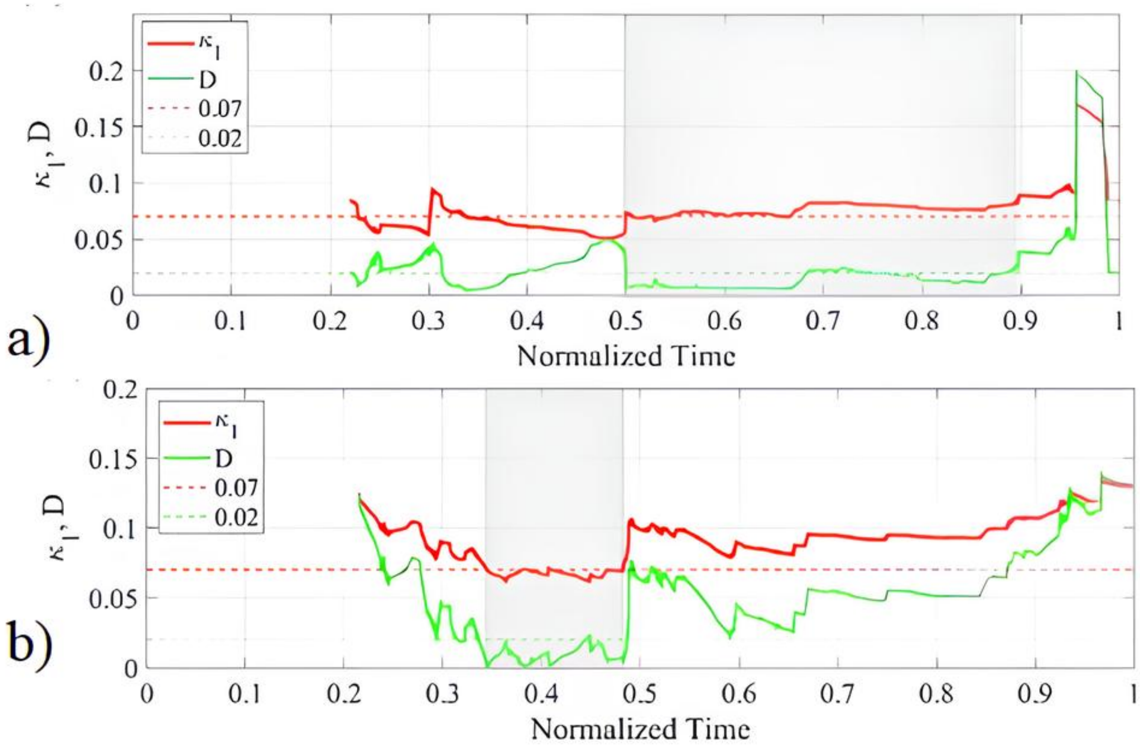

Figure 5: Comparison of the PCB and MEMS sensors: (a) PCB NT analysis considering $Q=A^{1.5}$; (b) MEMS NT analysis considering $Q=A^{1.5}$.

## 5. CONCLUSIONS

This study validated the use of MEMS-based AE monitoring in 3D-printed structures through comparative analysis with a commercial sensor. The b-value and Natural Time approaches confirmed the ability of MEMS sensors to track damage evolution and detect critical conditions. MEMS sensors captured high-frequency, high-energy events effectively, offering a cost-effective and scalable alternative for structural health monitoring.

## 6. ACKNOWLEDGEMENTS

The authors wish to acknowledge the support of the Brazilian National Council for Scientific and Technological Development (CNPq), the Coordination for the Improvement of Higher Education Personnel (CAPES), and the Research Support Foundation of the State of Rio Grande do Sul (FAPERGS), under grant numbers 22/2551-0000841-0 and 24/2551-0000772-5.

## 7. REFERENCES

AKI, K. (1967). Scaling law of seismic spectrum. *Journal of Geophysical Research*, 72(4), 1217–1231.

ANALOG DEVICES. (2024). Datasheet ADXL1002BCPZ. Available at: https://www.analog.com. Accessed on: 31 Aug. 2025.

CARPINTERI, A.; MANUELLO, A.; PUGNO, N. (2009). Evolution of the b-value. *Chaos, Solitons & Fractals*, 41(2), 843–853.

FRIEDRICH, L. F.; SILVA, R.; PEREIRA, T. (2021). AE in GFRP. *Composite Structures*, 256, 113105.

GUTENBERG, B.; RICHTER, C. F. (1944). Frequency of earthquakes in California. *Bulletin of the Seismological Society of America*, 34, 185–188.

KHAN, T. M.; ALI, S.; HUSSAIN, M. (2023). Multi-frequency MEMS acoustic emission sensor. *Sensors and Actuators A: Physical*, 362, 114648.

OZEVIN, D. (2020). MEMS Acoustic Emission Sensors. *Applied Sciences*, 10, 8966.

PCB PIEZOTRONICS. (2025). Product Datasheet: Model 352C03. Available at: https://www.pcb.com/products?m=352C03. Accessed on: 31 Aug. 2025.

SHIMADZU CORPORATION. (2025). Autograph AGS-X Series. Available at: https://www.shimadzu.com.br. Accessed on: 31 Aug. 2025.

VAROTSOS, P. A.; ALEXOPOULOS, K.; NOMIKOS, K.; SAMARIS, T. (2003). Natural Time Analysis: The New View of Time. Springer, Berlin.

SHIOTANI, T.; OHTSU, M.; KAMIYA, T. (1994). Evaluation of progressive failure using AE sources and improved b-value. *Progress in Acoustic Emission*, pp. 529–536.